

KIT SCIENTIFIC REPORTS 7672

Magnetoconvection in HCLL Blankets

C. Mistrangelo, L. Bühler

C. Mistrangelo, L. Bühler

Magnetoconvection in HCLL Blankets

Karlsruhe Institute of Technology
KIT SCIENTIFIC REPORTS 7672

Magnetoconvection in HCLL Blankets

by
C. Mistrangelo
L. Bühler

Impressum



Karlsruher Institut für Technologie (KIT)
KIT Scientific Publishing
Straße am Forum 2
D-76131 Karlsruhe

KIT Scientific Publishing is a registered trademark of Karlsruhe
Institute of Technology. Reprint using the book cover is not allowed.

www.ksp.kit.edu



*This document – excluding the cover – is licensed under the
Creative Commons Attribution-Share Alike 3.0 DE License*

(CC BY-SA 3.0 DE): <http://creativecommons.org/licenses/by-sa/3.0/de/>



*The cover page is licensed under the Creative Commons
Attribution-No Derivatives 3.0 DE License (CC BY-ND 3.0 DE):*

<http://creativecommons.org/licenses/by-nd/3.0/de/>

Print on Demand 2014

ISSN 1869-9669

ISBN 978-3-7315-0226-5

DOI: 10.5445/KSP/1000041270

Magneto-convection in HCLL blankets

Abstract

In the present work we consider magneto-convective flows in one of the proposed European liquid metal blankets that will be tested in the experimental fusion reactor ITER. Here the PbLi alloy is used as breeder material and helium as coolant. In order to finalize the design of the helium cooled lead lithium (HCLL) blanket, studies are still required to fully understand the behavior of the electrically conducting breeder under the influence of the intense magnetic field that confines the fusion plasma and in case of non-uniform thermal conditions. Liquid metal HCLL blanket flows are expected to be mainly driven by buoyancy forces caused by non-isothermal operating conditions due to neutron volumetric heating and cooling of walls, since only a weak forced flow is foreseen for tritium extraction in external ancillary systems. Buoyancy can therefore become very important and modify the velocity distribution and related heat transfer performance of the blanket.

The present numerical study aims at clarifying the influence of electromagnetic and thermal coupling of neighboring fluid domains on magneto-convective flows in geometries relevant for the HCLL blanket concept. According to the last design review two internal cooling plates subdivide the fluid domain into three slender flow regions, which are thermally and electrically coupled through common walls. First a uniform volumetric heat source is considered to identify the basic convective patterns that establish in the liquid metal. Results are then compared with those obtained by applying a realistic radial distribution of the power density as obtained from a neutronic analysis. Velocity and temperature distributions are discussed for various volumetric heat sources and magnetic field strengths.

MHD-Konvektion in HCLL Blankets

Zusammenfassung

In diesem Bericht werden magnetohydrodynamische Strömungen in einem Europäischen Flüssigmetallblanket für ITER untersucht, die durch thermische Auftriebskräfte hervorgerufen werden. Die flüssige Legierung PbLi wird hierbei als Brutmaterial verwendet und Helium dient als Kühlmittel. Für ein endgültiges Design eines heliumgekühlten Blei-Lithium - (helium cooled lead lithium, HCLL) - Blankets ist es nötig, das Verhalten des elektrisch leitenden Brutmaterials unter dem Einfluss des starken Magnetfeldes, das das Plasma einschließt, zu verstehen. Es ist zu erwarten, dass die Flüssigmetallströmungen hauptsächlich durch Auftriebskräfte aufgrund von Dichteunterschieden bei nicht-isothermen Betriebsbedingungen hervorgerufen werden. Diese entstehen durch die Wärmefreisetzung der Fusionsneutronen im Brutmaterial und durch Kühlung der Blanketwände. Die auftretenden Konvektionsströmungen können die Geschwindigkeitsverteilung und die Wärmeübertragung wesentlich beeinflussen. Die sehr schwache Zwangsströmung zur Abfuhr des erbrüteten Tritiums aus dem Blanket wird bei den betrachteten Beispielen vernachlässigt.

Die aktuellen numerischen Untersuchungen sollen den Einfluss der elektromagnetischen und thermischen Kopplung von benachbarten Fluidbereichen auf die Magnetokonvektion in HCLL-relevanten Blanketgeometrien klären. Entsprechend dem aktuellen Designkonzept wird jede Bruteinheit durch zwei interne Kühlplatten in drei flache Strömungsbereiche unterteilt, die über die Kühlplatten hinweg thermisch und elektrisch miteinander gekoppelt sind. Um einen ersten Einblick in die wesentlichen physikalischen Phänomene zu gewinnen, wird zunächst eine homogene volumetrische Wärmefreisetzung im Fluid betrachtet. Diese Ergebnisse werden anschließend mit Simulationen verglichen, bei denen realistische Leistungsprofile aus neutronischen Rechnungen zugrunde gelegt werden. In Abhängigkeit der eingebrachten Volumenheizung und des Magnetfeldes werden Ergebnisse für die Strömungs- und Temperaturverteilung vorgestellt.

Magneto-convection in HCLL blankets

Contents

1	Introduction	1
2	Governing equations and scaling	3
2.1	Wall heat transfer model	4
2.1.1	Validation of the heat transfer model	5
3	Numerical results	7
3.1	Infinitely extended horizontal ducts with uniform heat source	7
3.1.1	Two dimensional magneto-convection	7
3.1.2	Three dimensional MHD-buoyant flows	9
3.2	Cavity with non-uniform thermal loads	13
4	Conclusions	23
	References	25

1 Introduction

The Helium Cooled Lead Lithium (HCLL) blanket is being considered in Europe for testing in the international thermonuclear experimental reactor ITER. This blanket concept uses ferritic-martensitic steel (Eurofer) as structural material and an eutectic lead lithium alloy PbLi as breeder and neutron multiplier. As coolant helium with inlet/outlet temperature of 300/500°C is used. It flows in channels grooved into the walls and in parallel horizontal cooling plates (CP) located inside the breeder units (BU). The present design of the cooling system foresees the successive cooling of first wall, stiffening plates and cooling plates to remove the heat load generated by nuclear reactions. This ensures large outlet temperatures for high thermal efficiency (Aiello, de Dinechin, Forest, Gabriel, Li Puma, Rampal, Rigal, Salavy and Simon (2011)). The temperature of the structural material has to be kept within suitable limits, represented by a minimum value of about 300°C, determined by embrittlement conditions of Eurofer under irradiation, and by a maximum value of 550°C set by the creep strength.

A HCLL blanket module consists of a rectangular box reinforced by an array of stiffening plates (SP) that create a grid of rectangular cells where breeder units are positioned in which PbLi flows with velocities of the order of $0.1 \div 1$ mm/s (Salavy, Aiello, David, Gabriel, Giancarli, Girard, Jonquieres, Laffont, Madeleine, Poitevin, Rampal, Ricapito and Splichal (2008)). This weak forced flow is required to transport PbLi towards external ancillary systems for purification and tritium extraction. Due to the small imposed velocities it is expected that the liquid metal flow in the blanket is mainly driven by buoyancy forces caused by non-uniform thermal conditions resulting from neutron heat generation in the liquid metal and cooling of walls.

Velocity distributions inside the blanket are significantly influenced by the magnetic field that confines the fusion plasma. In case of intense applied magnetic fields the main balance of forces establishes between buoyant and electromagnetic forces induced by the interaction of electric currents with the magnetic field. The latter forces weaken the convective flow compared to hydrodynamic conditions. The intensity of the magnetohydrodynamic (MHD) damping depends on the strength of the magnetic field and on its orientation with respect to the convective circulation. The resulting magneto-convective flow is characterized by interesting flow patterns that affect the temperature distribution and tritium transport in BUs and therefore the thermal performance of the blanket.

Numerical modeling of magneto-convection flows relevant for fusion applications requires to consider both the power generation in the liquid metal and the heat extraction through the helium-cooled walls. The complex paths of electric currents in the fluid and in the electrically conducting structure have to be modeled as well.

In the past various studies have been performed to analyze convection in differentially heated cavities for different orientations of the magnetic field (Ozoe and Okada (1989), Ben Hadid and Henry (1997), Gelfgat and Molokov (2011)). Fundamental MHD buoyant flows have been studied in simplified geometries. For instance MHD flows in electrically conducting vertical ducts with uniform volumetric heating and heat extraction through walls parallel to the magnetic field have been investigated by means of an asymptotic method valid for inertialess flows and large applied magnetic fields (Bühler (1998)). The established velocity distribution is characterized by downward jets at walls aligned with the magnetic field and an upward 3D core flow.

Very few studies are available in case of MHD buoyant flow in horizontal channels with internal volumetric sources and for control parameters relevant for fusion blanket applications. Analysis of steady state MHD convective flows for applications to HCLL blankets have been

carried out for instance by Kharicha, Molokov, Aleksandrova and Bühler (2004), where closed electrically conducting cavities with a radially varying internal heat source were considered. It was observed that in such a blanket configuration the intensity of the buoyant flow can become comparable to the forced one. Other applied studies of buoyant MHD flow in simplified HCLL blanket-related geometries with neutron power source and in case of insulating or perfectly conducting walls have been presented in Mas de Les Valls, Batet, de Medina, Fradera and Sedano (2011). The same authors concluded that fluid-solid thermal coupling is required to accurately predict the complex structure of the magneto-convective flows in HCLL blankets (Mas de les Valls, Batet, de Medina and Sedano (2012)). Mixed convection MHD flows with volumetric heating have been investigated for dual coolant blanket applications in long vertical ducts with thermally and electrically insulating walls by Vetcha, Smolentsev, Abdou and Moreau (2013).

In the present report we discuss results from 2D and 3D numerical simulations of liquid metal MHD flows in geometries related to a breeder unit of a HCLL blanket with internal power generation and heat extraction through the helium-cooled walls. The influence of pure natural convection is investigated neglecting the effects of the weak forced flow. We take simultaneously into account real electric and thermal properties of the walls and the presence of a uniform and a spatially varying volumetric heat source in the liquid metal as given by neutronic analyses Villari, Petrizzi and Moro (2010). Dimensions, material properties and basic operating conditions are taken according to the most recent description of the reference HCLL test blanket module (TBM) for ITER (Aiello et al. (2011), Rampal, Aiello and Li Puma (2009)). The main effect of imposing a magnetic field on a liquid metal flow is the alignment of convective flow patterns with the field lines. This has been already observed for instance in case of Rayleigh–Bénard MHD convection (Burr and Müller (2002)). An interesting phenomenon that has not been considered yet is the full thermal and electromagnetic coupling of flows in sub-channels that form the blanket module, caused by the finite electric and thermal conductivity of the walls.

Results for two different problems are summarized in this report. First we consider horizontal slender ducts that are infinitely extended in radial direction and where a thermal source is uniformly distributed in the fluid. All the volumetric heat supplied to the liquid metal is extracted homogeneously through the walls to simulate cooling by helium. This kind of simplified problem is investigated to identify convective patterns that establish inside the channels when the thermal load is sufficiently large and the basic conductive state loses its stability. It is interesting to observe how the convective rolls change their shape and number by increasing the volumetric heating. Moreover, the influence of the thermal coupling between adjacent fluid domains, as present in a breeder unit of an HCLL blanket, is investigated.

The second problem is more complex. Magneto-convective flows in a cavity are studied where the influence of the presence of back plate and first wall on temperature and velocity distributions is taken into account. Uniform and radially varying thermal loads are applied and a model is derived to describe the heat exchange from the hot wall into the helium flow. An analytical solution for MHD flows between parallel infinitely extended vertical plates with volumetric heat source in the fluid has been developed and used to validate the heat transfer model.

2 Governing equations and scaling

We investigate liquid metal flows in a strong magnetic field in electrically and thermally conducting horizontal ducts where temperature gradients are present. The motion is affected by electromagnetic and buoyancy forces. Non-homogeneous thermal conditions are caused by internal volumetric heat sources that are distributed within the fluid and by heat extraction through the walls. Figure 1(a) shows details of the geometry considered. It consists of three flat channels like those that form a breeder unit of a HCLL blanket (Fig.1(b)). The dimensions and properties of fluid and wall materials are taken according to the latest design of a HCLL test blanket module (Aiello et al. (2011)). The thickness of the walls has been adapted to represent an average thermal and electric conductance equivalent to the one of real plates with internal helium channels.

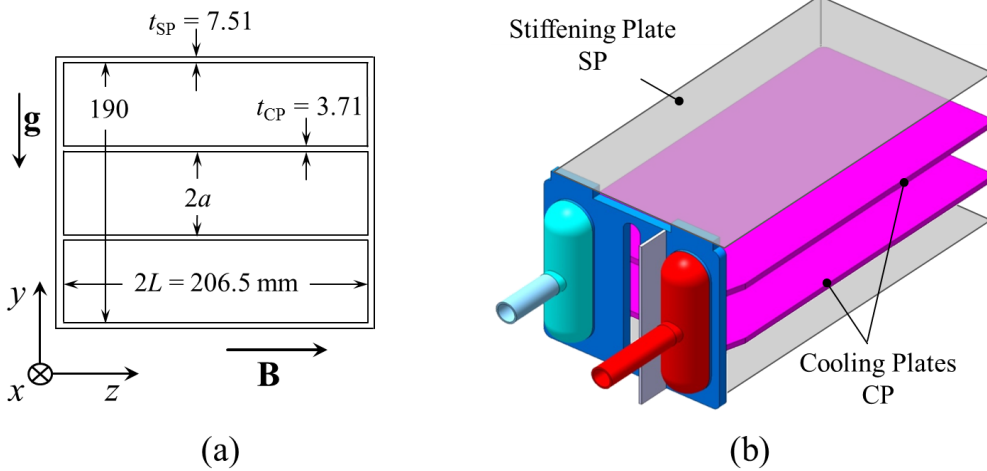


Figure 1: (a) Geometry used for numerical simulations. (b) Design of a breeder unit of a HCLL test blanket module.

Density changes due to temperature variations, which cause convective motions, are described by the Boussinesq approximation, which states that the fluid density is a linear function of temperature in the gravitational body force term, $\rho\beta(T - T_0)\mathbf{g}$, and constant elsewhere. Here ρ is the density at the reference temperature T_0 , β the volumetric thermal expansion coefficient and $\mathbf{g} = -g\hat{\mathbf{y}}$ the gravitational acceleration. The equations governing the problem are those accounting for balance of momentum, conservation of mass and charge. Ohm's law is used for computing electric current density. In non-dimensional form the equations can be written as (Bühler (1998)):

$$\frac{Gr}{Ha^4} \left(\frac{\partial}{\partial t} + \mathbf{v} \cdot \nabla \right) \mathbf{v} = -\nabla p + \frac{1}{Ha^2} \nabla^2 \mathbf{v} + \mathbf{j} \times \mathbf{B} + T\hat{\mathbf{y}}, \quad (1)$$

$$\nabla \cdot \mathbf{v} = 0, \quad \nabla \cdot \mathbf{j} = 0, \quad \mathbf{j} = -\nabla \phi + \mathbf{v} \times \mathbf{B}. \quad (2)$$

The dimensionless quantities \mathbf{B} , \mathbf{j} and ϕ represent magnetic induction, current density and electric potential, scaled by the magnitude of the applied magnetic field B_0 , by $\sigma v_0 B_0$ and $v_0 B_0 a$,

respectively. The non-dimensional pressure p is the difference between local and isothermal hydrostatic pressure, normalized by $\sigma v_0 B_0^2 a$. The characteristic velocity v_0 is chosen such that buoyant and electromagnetic forces balance each other, $v_0 = \rho \beta g \Delta T / (\sigma B^2) = (\nu/a) Gr_a / Ha_a^2$ (Hjellming and Walker (1987)). The physical properties of fluid and walls like electrical conductivity σ , thermal conductivity k , thermal diffusivity α and kinematic viscosity ν , are assumed to be constant in the temperature range considered and they are taken according to Jauch, Karcher, Schulz and Haase (1986). The control parameters of the problem are the Hartmann number Ha_a and the Grashof number Gr_a :

$$Ha_a = B_0 a \sqrt{\frac{\sigma}{\rho \nu}}, \quad (3)$$

$$Gr_a = \frac{g \beta \Delta T a^3}{\nu^2} = \frac{g \beta \bar{Q} a^5}{k \nu^2}. \quad (4)$$

The former one is proportional to the strength of the applied magnetic field and its square quantifies the relative importance of electromagnetic and viscous forces. The Grashof number Gr_a gives a measure for the ratio of buoyant and viscous effects and it is proportional to the average volumetric heat source \bar{Q} in the fluid. The dimensionless temperature T is given by $(T^* - T_0) / \Delta T$, where T^* is the local dimensional temperature and $\Delta T = \bar{Q} a^2 / k$ is a characteristic temperature difference. As a typical length scale a we use half of the height of a flat duct (Fig.1), since the vertical direction is aligned with gravity and the main heat transfer that determines ΔT occurs in y direction. In MHD studies the Hartmann number is typically defined with a characteristic dimension L measured along magnetic field lines, the so called Hartmann length. Therefore we introduce additionally the parameter

$$Ha = B_0 L \sqrt{\frac{\sigma}{\rho \nu}} = \frac{L}{a} Ha_a, \quad (5)$$

to facilitate the comparison with previous analyses. The distribution of temperature T in the fluid is given by the non-dimensional energy balance equation

$$Pe \left(\frac{\partial T}{\partial t} + (\mathbf{v} \cdot \nabla) T \right) = \nabla^2 T + q, \quad (6)$$

where $Pe = Gr_a / Ha_a^2 Pr$ is the Peclet number and $Pr = \nu / \alpha$ is the Prandtl number. The latter one is small for liquid metals ($Pr \simeq 0.03$ for PbLi at a temperature of 573K). In (6) q is obtained by scaling the volumetric heat source with $k \Delta T / a^2$.

The present study considers ducts with walls of finite thermal and electric conductivity. Therefore equations are solved both in the liquid metal and in the solid domain and they are coupled by suitable interface conditions. The latter ones state the continuity of electric potential, $\phi = \phi_w$, normal component of current density, $j_n = j_{n,w}$, temperature, $T = T_w$, and heat flux, $k \partial T / \partial n = k_w \partial T_w / \partial n$. The no slip condition is assumed at all walls, $\mathbf{v} = 0$, and the external surface of the walls is electrically and thermally insulating ($\partial \phi_w / \partial n = 0$, $\partial T_w / \partial n = 0$).

2.1 Wall heat transfer model

In this report two types of wall heat transfer models have been applied. In the first case considered, where MHD flows in infinitely long channels are simulated, a simplified model for

the wall heat extraction is used. The uniform volumetric thermal load released in the fluid is removed by homogeneously distributed heat sinks in the walls, representing the simplest model for the helium cooling. In the second case heat extraction depends on the local wall temperature and the thermal transport from the wall into the helium flow is described by the Gnielinski correlation as explained in the following.

In the wall the heat is extracted by helium flowing in a large number of tiny channels. In order to avoid numerical resolution of helium domains, the heat transfer to a unit area of helium-wall interface is determined as $\alpha (T_w - T_m)$, where α is the average value of the heat transfer coefficient and T_m is the mean coolant temperature $T_m = (T_e + T_i) / 2$ between the exit and inlet temperature values T_e and T_i . The heat which is removed by all cooling ducts in a unit volume of a wall is then given by $s\alpha (T_w - T_m)$, where s denotes the specific heat transfer surface of helium channels. As a result, the heat transfer from the hot wall into the helium flow is given by a volumetric (source/sink) term and the wall temperature T_w is calculated by the following equation

$$\rho_w c_{pw} \frac{\partial T_w}{\partial t} - k_w \nabla^2 T + s\alpha (T_w - T_m) = 0. \quad (7)$$

The thermal exchange from the hot walls to an assumed fully established helium flow, given in terms of the nondimensional Nusselt number Nu , can be described by the Gnielinski correlation for smooth tubes (Gnielinski (1975))

$$Nu = \alpha \frac{d}{k} = \frac{(\xi/8) (Re - 1000) Pr}{1 + 12.7 \sqrt{\xi/8} (Pr^{2/3} - 1)}, \quad (8)$$

where $\xi = (1.82 \lg Re - 1.64)^{-2}$ approximates the friction factor for a helium flow with given Reynolds and Prandtl numbers

$$Re = \frac{\bar{v} d}{\nu}, \quad Pr = \frac{\nu}{k/(\rho c_p)}. \quad (9)$$

Here d is an equivalent diameter of the cooling ducts in a considered wall and \bar{v} is the helium average velocity. The mean value of the heat transfer coefficient is then defined as $\alpha = Nu k/d$ and the wall heat flux is given by $\dot{q} = \alpha \Delta T_{in} \simeq \alpha (T_w - T_m)$. We select the Gnielinski approximation for the description of the heat transfer in TBM cooling channels in accordance with specifications of input data and physical correlations for the design of the HCLL TBM given in Rampal et al. (2009). The helium characteristic parameters, the Prandtl number, $Pr = 0.64$, and the Reynolds numbers, $2300 < Re < 10^6$, fit in the parameter range in which this correlation is valid (see Table 1). Wall and coolant properties are taken at the mean He temperature T_m (Rampal et al. (2009), Tavassoli (2004), Mergia and Boukos (2008)) and local thermal effects when He enters the coolant channels are neglected since the channels are very long in comparison to their cross section dimensions.

2.1.1 Validation of the heat transfer model

Calculations have been performed by using a numerical solver developed in the finite volume code OpenFOAM for accurate numerical simulation of 3D incompressible, viscous flows of electrically conducting fluids, e.g. liquid metals, exposed to an externally imposed magnetic field (Mistrangelo and Bühler (2011)). The current density conservative scheme proposed in Ni,

Munipalli, Morley, Huang and Abdou (2007) is employed and pressure–velocity coupling is accomplished by a PISO (Pressure Implicit with Splitting of Operators) algorithm, the central difference scheme has been used for spatial discretization.

In order to validate the heat transfer model used to describe thermal exchange in fluid and heat extraction through the walls, an analytical solution has been developed that describes a simplified model problem consisting of buoyant MHD flow between two infinitely extended parallel vertical plates perpendicular to an imposed magnetic field (Fig.2(a)). The fluid is heated by a uniform volumetric heat source.

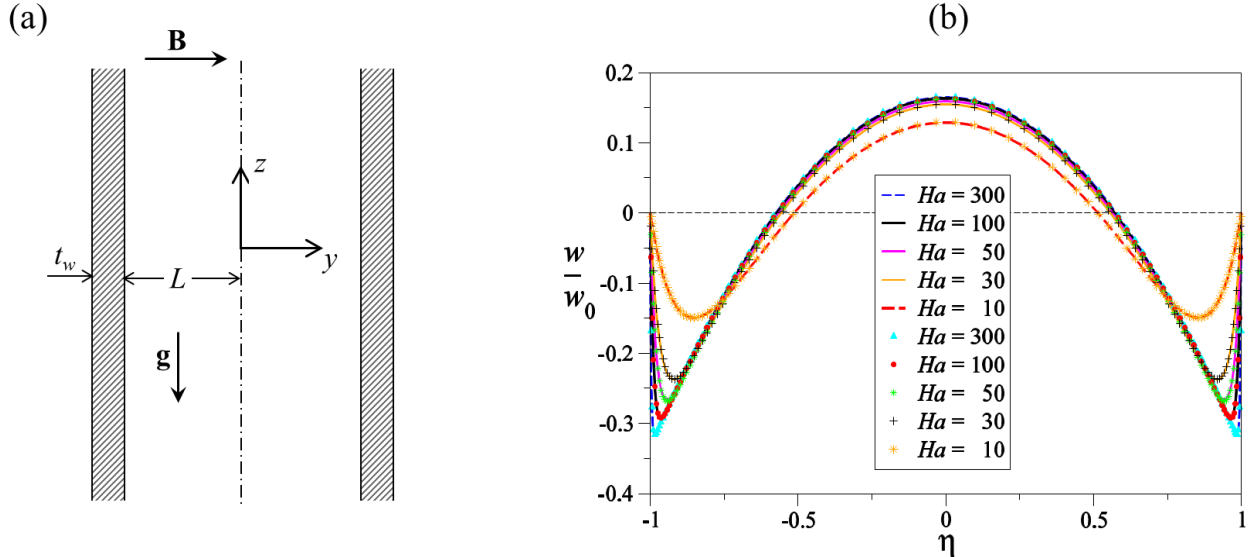


Figure 2: (a) Sketch of the geometry and reference system used for validation of the heat transfer model. (b) Distribution of the scaled vertical velocity w/w_0 along the magnetic field direction $\eta = y/L$ for different Hartmann numbers Ha . Symbols indicate the numerical results and lines the analytical solution.

In Fig.2(b) the normalized vertical velocity w/w_0 is plotted along the scaled magnetic field direction $\eta = y/L$ for various Hartmann numbers Ha . Numerical results are marked by symbols and the analytical solution by solid lines. It can be seen that for strong magnetic fields ($Ha \gg 1$) the velocity distribution consists of a parabolic core profile and thin Hartmann boundary layers at walls perpendicular to the magnetic field at $\eta = \pm 1$. The thickness of the Hartmann layers reduces by increasing Ha , i.e. for stronger magnetic fields. The stationary solutions plotted in Fig.2(b) are independent of the Grashof number in the velocity scale considered, where a characteristic velocity w_0 is chosen such that buoyant and electromagnetic forces balance each other, $w_0 = \rho\beta g\Delta T/(\sigma B_0^2)$ (Hjellming and Walker (1987)). The agreement between numerical solutions and analytical results is excellent.

3 Numerical results

3.1 Infinitely extended horizontal ducts with uniform heat source

The results discussed aim at explaining the influence of thermal and electric coupling of neighboring fluid domains on magneto-convective patterns, as it occurs in case of ducts formed between cooling (CP) and stiffening (SP) plates (see Fig.1). We investigate flows at large Hartmann numbers ($Ha \geq 2000$) and for Grashof numbers Gr_a in a range corresponding to volumetric heating of $0.04 \div 5 \text{ MW/m}^3$. The order of magnitude of the selected heat sources is close to average values expected in HCLL (Gabriel, Escuriol, Dabbene, Gastaldi, Salavy and Giancarli (2007)) and DCLL (Sawan, Marriott and Dagher (2009)) blanket modules. We investigate first 2D buoyant MHD flows with the purpose of understanding the basic flow state. Then we consider ducts with a large axial extent where 3D disturbances in the temperature field can develop. For these two set-ups we analyze the MHD flow both in a single duct and in three thermally and electrically coupled channels as shown in Fig.1(a). It is assumed that the considered breeder unit is part of a blanket module and therefore, walls that are common to two fluid domains are taken with half of their actual thickness.

3.1.1 Two dimensional magneto-convection

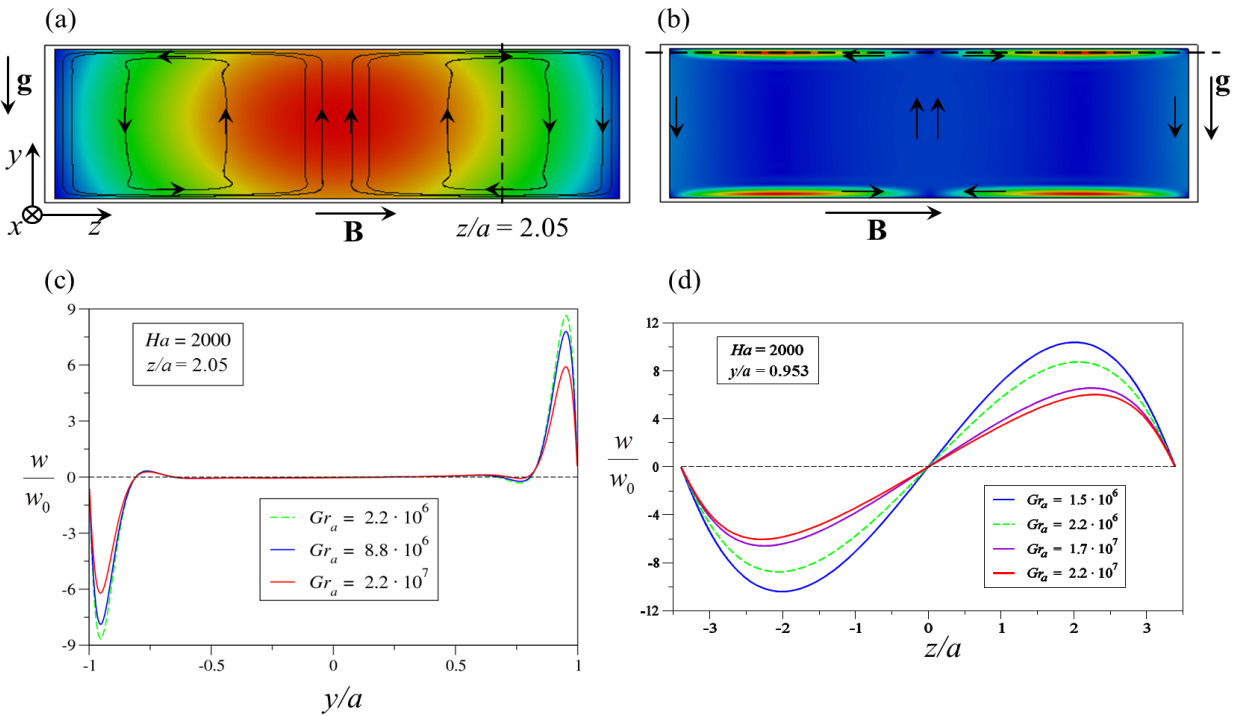


Figure 3: (a) Contours of temperature and velocity streamlines, and (b) magnitude of the velocity in the duct cross-section for MHD-buoyant flow at $Ha = 2000$ and $Gr_a = 2.2 \cdot 10^6$. In (c) the z -component of the scaled velocity is plotted along the vertical line at $z/a = 2.05$ and in (d) along the line at $y/a = 0.953$ in the side layer.

In Fig.3(a) contours of temperature are depicted in the duct cross-section for the MHD-buoyant flow at $Ha = 2000$ and $Gr_a = 2.2 \cdot 10^6$ ($\bar{Q} \simeq 0.03$ MW/m³). For this small Grashof number the vertical temperature profile $T(y)$ is almost symmetric and very close to a parabolic shape with the maximum slightly shifted towards the upper stiffening plate. This results from the weak convective motion driven by the horizontal temperature gradient. Velocity streamlines are plotted in the duct cross-section showing the flow circulation. The warmer fluid in the core of the duct experiences an upward buoyancy force and moves towards the upper wall. Near the Hartmann walls, perpendicular to \mathbf{B} , the temperature reduces and the fluid sinks. Strong velocities are present in the side layers at walls parallel to the magnetic field as shown by the contours of the velocity magnitude in Fig.3(b). In Fig.3(c)-(d) the normalized z - component of the velocity is plotted along the vertical line at $z/a = 2.05$ and along the horizontal line at $y/a = 0.953$, respectively, for various Grashof numbers. The velocity distribution described corresponds to a stable steady state configuration where even in the upper part of the duct, where an unstable thermal stratification is present, small perturbations are suppressed by the combined stabilizing effect of viscosity in the parallel layer, MHD-damping and heat conduction. Electric currents, induced by the interaction of the vertical velocity with the imposed magnetic field, flow in positive axial direction in the center of the duct where the fluid moves upwards and in negative direction in regions close to the Hartmann walls where the liquid metal descends. No electric potential variation occurs in the channel and as a result there is no current flowing in the walls. By increasing the volumetric heating the maximum of the temperature distribution moves closer to the top stiffening plate that becomes warmer compared to the lower one owing to the stronger convective heat flux.

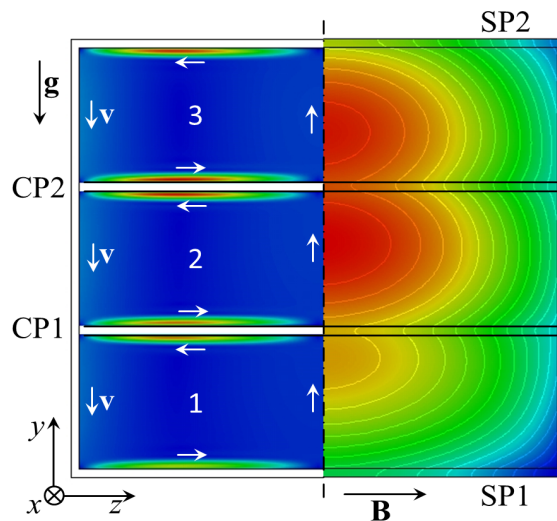


Figure 4: Contours of velocity magnitude (left) and temperature distribution (right) in three thermally and electrically coupled ducts for 2D buoyant-MHD flow at $Ha = 2000$ and $Gr_a = 8.8 \cdot 10^6$.

In geometries related to liquid metal blankets like the one shown in Fig.1, the temperature distribution is significantly affected by the thermal coupling between the parallel channels. In Fig.4 contours of temperature are shown on the right in half of the geometry. A large temperature difference occurs between the two stiffening plates SP1 and SP2 as well as between

the bottom wall SP1 and the cooling plate CP1. In the lower duct a stable thermal stratification occupies almost all the channel height, while large unstable regions are present in ducts 2 and 3 near CP2 and SP2, respectively. The higher temperature in the central duct is caused by the fact that the cooling plates are thinner than the stiffening plates and they are shared by two channels, i.e. they receive heat from two sides. The non-homogeneous temperature distribution results from the intense thermal coupling of the ducts. As a consequence also the velocity distribution becomes asymmetric as shown in Fig.4 on the left. Here contours of the velocity magnitude are displayed. The circulation in the lower duct is much weaker than in the other two. It is interesting to notice that in case of isothermal MHD forced flows the electric coupling was so strong that the cooling plates behaved practically as perfectly conducting (Mistrangelo and Bühler (2008)). Here in addition the thermal coupling is important. For larger heat sources the temperature difference between the horizontal stiffening plates becomes larger and larger. However, it should be noted that the described 2D flow becomes unstable if Gr_a exceeds a critical value $Gr_{a,cr}$. For $Gr_a > Gr_{a,cr}$ three dimensional disturbances develop as described in the next section.

3.1.2 Three dimensional MHD-buoyant flows

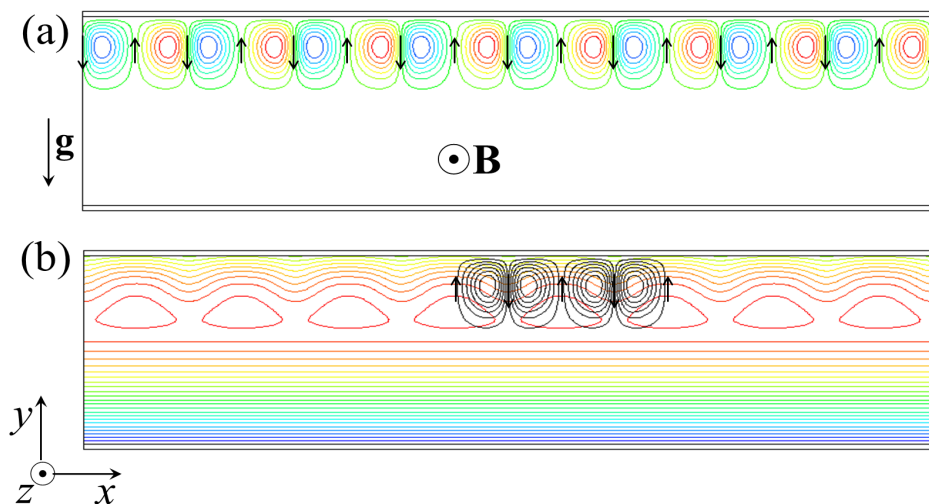


Figure 5: Buoyant MHD flow at $Ha = 2000$ and $Gr_a = 2.2 \cdot 10^7$ in a horizontal channel with constant volumetric heating. (a) Contours of electric potential in the middle plane $z = 0$. (b) Isotherms with a non-dimensional distance of 0.023.

Let us consider now 3D magneto-convective flows in a single duct that is infinitely extended in radial (x) direction, so that axial disturbances in the temperature field can develop and propagate. If the volumetric heat source is smaller than a critical value ($Gr_a < Gr_{a,cr}$), a stable steady regime independent of x , as described by 2D simulations (see section 3.1.1), establishes. By increasing the internal heating, i.e. the Grashof number, perturbations develop in the upper half of the duct, where an unstable thermal stratification is present, and a well organized convective motion sets in in the form of convective rolls with axes aligned with the magnetic field. Those convective cells are superimposed on the weaker 2D circulation, which occurs on

yz - planes, caused by the horizontal component of temperature gradient that results in jets in the parallel layers (see e.g. contours of velocity magnitude in Fig.3(b) and Fig.4(left)). In Fig.5(a) contours of electric potential are plotted on a middle plane of the duct at $z = 0$ for the flow at $Ha = 2000$ and $Gr_a = 2.2 \cdot 10^7$ ($\bar{Q} \simeq 0.3 \text{ MW/m}^3$). They clearly show the structure of the convective rolls that develop as pairs of counter-rotating cells. Arrows indicate the direction of rotation. The velocity of the descending fluid is larger than the one of the ascending flow. In Fig.5(b) isolines of temperature are depicted on the same plane at $z = 0$. In the lower half of the duct, where isotherms are horizontal and parallel, there is a stable thermal stratification and in the upper part temperature disturbances grow as a result of the convective heat transfer. For the present set of control parameters, the temperature along the upper stiffening plate can be 20 degrees higher than the one at the lower plate. This difference increases significantly for larger heat sources. In Fig.5(b) two pairs of rotating cells are displayed, superimposed on the temperature isolines: the ascending flow is indicated by the fact that the isotherms near the upper wall are more compacted.

Simulations performed for larger Hartmann numbers, i.e. for more intense magnetic fields, not explicitly presented here, show the stabilizing effect of MHD damping, which leads to a more homogeneous temperature and velocity distribution when the same volumetric heating is imposed. The stabilizing effect of the magnetic field was already observed in case of Rayleigh–Bénard convection (Burr and Müller (2002)). A detailed investigation is planned to identify the non-dimensional parameter that governs the onset of the convective rolls and to study systematically the influence of increasing and spatially varying heat sources on local velocity and wall temperature gradients.

Figure 6(a) shows a 3D view of the regular convective rolls in the duct by means of iso-surfaces of electric potential, colored by temperature. Some velocity streamlines are plotted in Fig.6(b). The largest velocities are localized in the layers that form along the upper and lower walls parallel to the magnetic field. Outside these parallel layers, in the region that has a stable density stratification, only a very weak flow occurs. Near the top SP the fluid moves horizontally along z towards the Hartmann walls, and close to the bottom plate towards the middle plane of the duct. A second fluid circulation that has the form of the above described convective rolls is superimposed on the 2D motion sketched in Fig.3(a).

For higher Grashof numbers the amplitude of spatially periodic temperature disturbances becomes larger and the convective motion gradually grows deeper into the duct and destroys the underlying stable density stratification. This is displayed in Fig.7 where temperature and electric potential contours are plotted for flows at $Ha = 2000$ and increasing Grashof numbers. All those results show the first 3D regime that is characterized by periodic convective rolls.

By further increasing the volumetric heat source a transitional convective pattern occurs that leads to a second 3D regime where larger and irregular cells are present (see Fig.8). It is therefore possible to identify a certain critical value of the Grashof number beyond which the convective rolls lose their periodicity, they increase in size and then they become time dependent. The transition regime is characterized by the elongation of pairs of rolls and the subsequent merging of cells to form bigger structures.

Similar flow features as for single ducts are found when considering electrically and thermally coupled ducts as shown in Fig.9 for the flow at $Ha = 2000$ and two Grashof numbers Gr_a . On the left, isotherms are shown on the plane $z = 0$. In the lower and in the middle channels the temperature field is stable even where an unstable density stratification is present. Perturbations

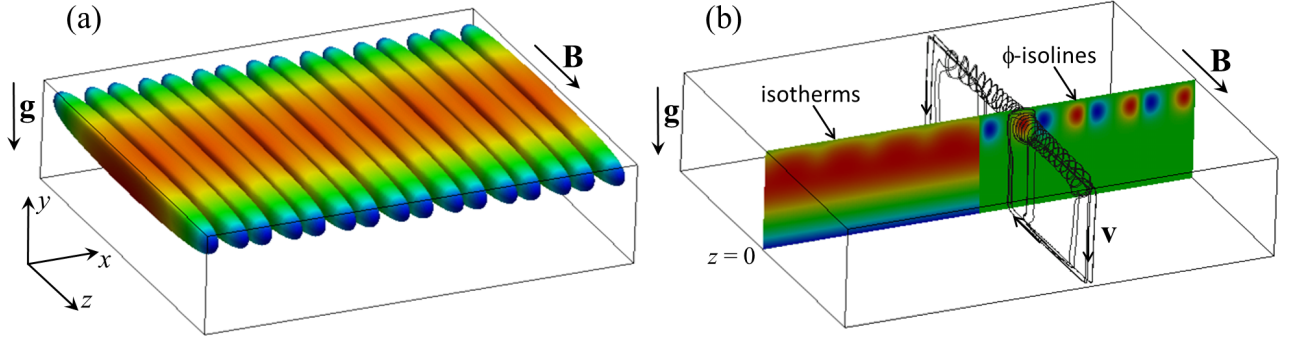


Figure 6: Flows at $Ha = 2000$ and $Gr_a = 2.2 \cdot 10^7$. (a) Isosurfaces of potential are used to visualize the convective rolls. They are colored by the temperature. (b) Temperature (left) and electric potential (right) on the plane at $z = 0$. Some 3D velocity streamlines are shown in black.

in the temperature field are instead visible in a large portion of the upper duct. The occurrence of convective rolls is displayed in Fig.9 on the right by means of contours of electric potential. In the middle and lower channels the potential is zero, no convective motion occurs and the heat transfer is due exclusively to conduction. It can be observed that by rising Gr_a the number of convective cells increases.

In Fig.10 isotherms and potential isolines are displayed for the flow at $Ha = 2000$ and $Gr_a = 1.7 \cdot 10^7$ ($\bar{Q} \simeq 0.26 \text{ MW/m}^3$). Electric potential isolines are plotted on the plane $z = 0$ only in the upper duct, since in the other two channels the potential is zero. Isotherms are instead depicted in the lower and middle channels where even in the regions with unstable stratification no perturbations develop. In the top duct temperature isolines are qualitatively as in Fig.7 (top left) for the flow in a single channel with the same volumetric heating. In this coupled geometry there are 12 pairs of convective rolls, while in a single duct for the same heat source only 8 cells are present. For all the cases discussed above convective motion develops in the upper duct in the form of periodic rolls.

If we consider a larger volumetric heating ($Gr_a = 2.2 \cdot 10^7$) equal to the one applied in the case of a single duct previously described (see Fig.6), the established convective pattern is more complex as visualized by the potential iso-surfaces in Fig.11(a). In the upper duct large irregular structures are present while in the middle channel smaller periodic convective rolls develop. This is visualized by isotherms and isolines of potential on the plane $z = 0$ displayed in Fig.11(b)-(c). The fluid in the lower duct is still stable. By increasing further the heat source, temperature perturbations extend also to the last duct. A more detailed description of the evolution of the convective cells is the subject of ongoing investigations.

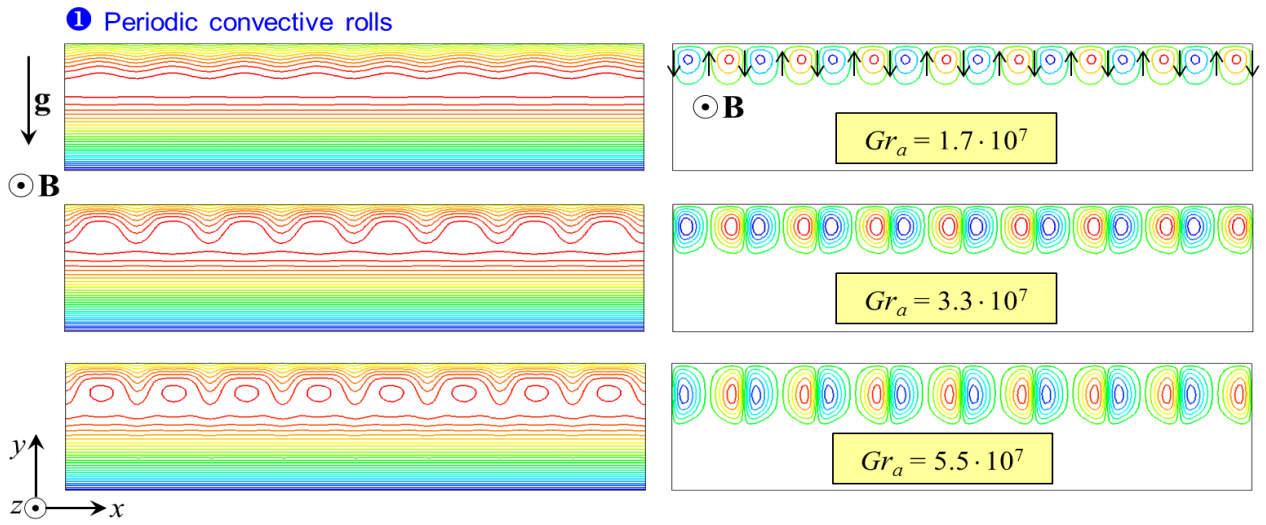


Figure 7: On the left contours of temperature with non-dimensional distance of 0.02 and on the right electric potential contours, indicating approximate streamlines, with a non-dimensional distance of 0.12. Flow at $Ha = 2000$ and increasing Grashof numbers.

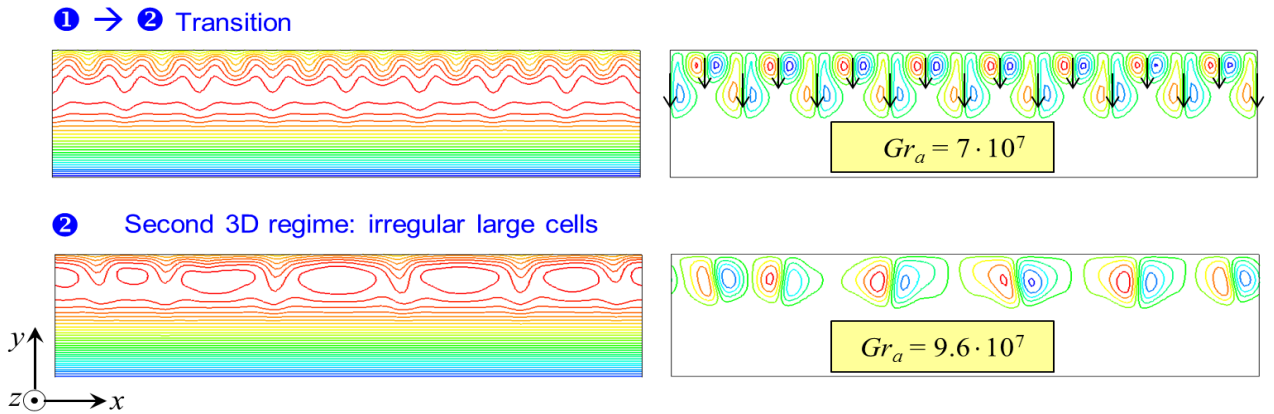


Figure 8: Temperature (left) and electric potential contours (right) for the flow at $Ha = 2000$ and large Grashof numbers, showing the transition from the first 3D regime to the second one.

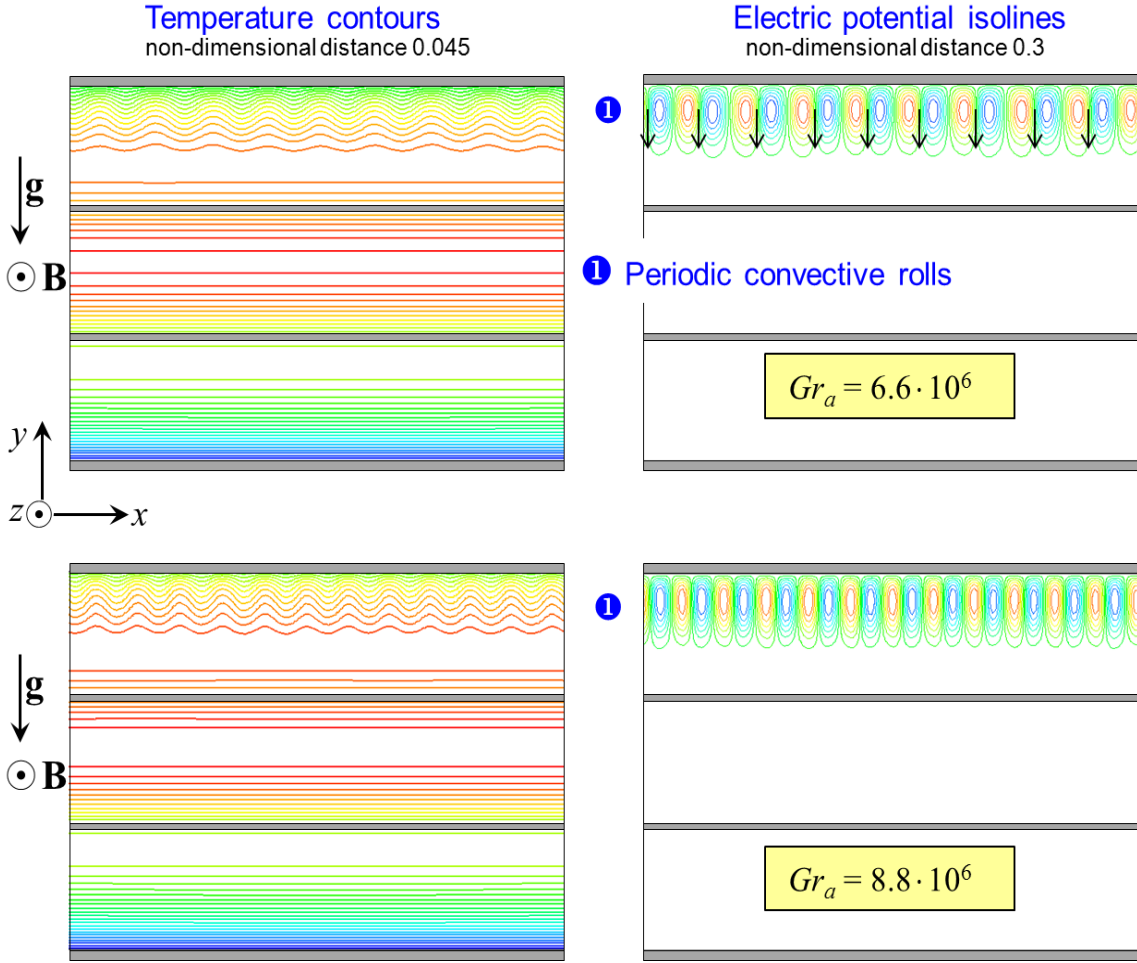


Figure 9: Flow at $Ha = 2000$ and two different Grashof numbers Gr_a in three coupled long ducts. Temperature (left) and electric potential (rights) isolines are plotted on the plane $z = 0$.

3.2 Cavity with non-uniform thermal loads

Magneto-convective flows are studied in a breeder unit of a HCLL blanket module. As a model geometry the available design of a HCLL TBM for ITER has been chosen. Here two cooling plates are present which subdivide the fluid domain in three slender channels that we will refer to as ch1, ch2 and ch3 as shown in Fig.12.

Thermal exchange in the helium cooling ducts has been simulated by means of the model described in section 2.1. The main parameters used to determine heat transfer coefficients are taken from a thermal-hydraulic analysis of a BU (LiPuma, Aiello and Morin (2010)) and summarized in Table 1.

Data from a neutronic analysis for the HCLL TBM, where radial profiles of nuclear heating in different blanket constituent materials are determined, has been used as input for the distribution of the thermal source in the liquid breeder (Villari et al. (2010)). The radial power density distribution varies from a maximum of about 5 MW/m^3 at the first wall to a minimum of 0.2 MW/m^3 at the back plate. A surface wall heat flux of 0.3 MW/m^2 is applied at the first

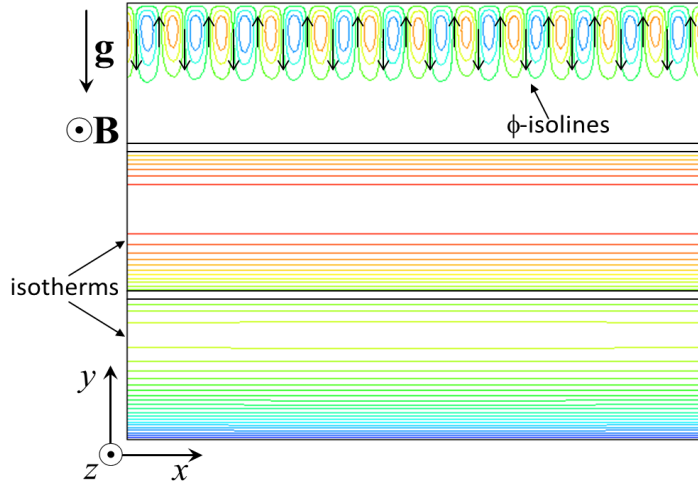


Figure 10: Flow at $Ha = 2000$ and $Gr_a = 1.7 \cdot 10^7$ in three coupled long ducts. Electric potential isolines are plotted on the plane $z = 0$ in the upper duct and isotherms in the two lower channels.

wall (average value during D – T phase in ITER). Results for MHD flows in a BU with uniform volumetric heat load are also considered for comparison.

In the following, the buoyant flow resulting from the non-uniform thermal conditions caused by a constant internal volumetric heating $\bar{Q} = 1 \text{ MW/m}^3$ ($Gr_a = 0.85 \cdot 10^8$) and heat extraction through the walls is considered. For these conditions the solution is time-dependent. The main global flow features are presented in terms of time-averaged quantities and magnitude of fluctuations. In Fig.13 iso-surfaces of time-averaged electric potential are used to visualize the convective patterns. Contours are colored by the mean temperature and results are obtained for a constant Hartmann number $Ha = 1000$. Along the first wall (FW) there is a strong downward flow due to the low helium temperature ($T_m = 344.5^\circ\text{C}$) in this wall, which is the first cooled element in the proposed helium circuit for the HCLL TBM (Aiello, Gabriel, Rampal and Salavy (2009)). Moreover, in this study the neutronic heat generation in the wall is not taken into account. The occurrence of a thermal load in the walls will be considered in a next

	CP	SP	FW
$T_m [^\circ\text{C}]$	481.5	433	344.5
Re	$8.15 \cdot 10^3$	$1.02 \cdot 10^4$	$2.5 \cdot 10^5$
Pr	0.639	0.639	0.639
Nu	23.5	29	365
$\alpha \left[\frac{\text{W}}{\text{m}^2\text{K}} \right]$	1656.3	1102	6326.67

Table 1: Helium parameters used to define heat transfer coefficients.

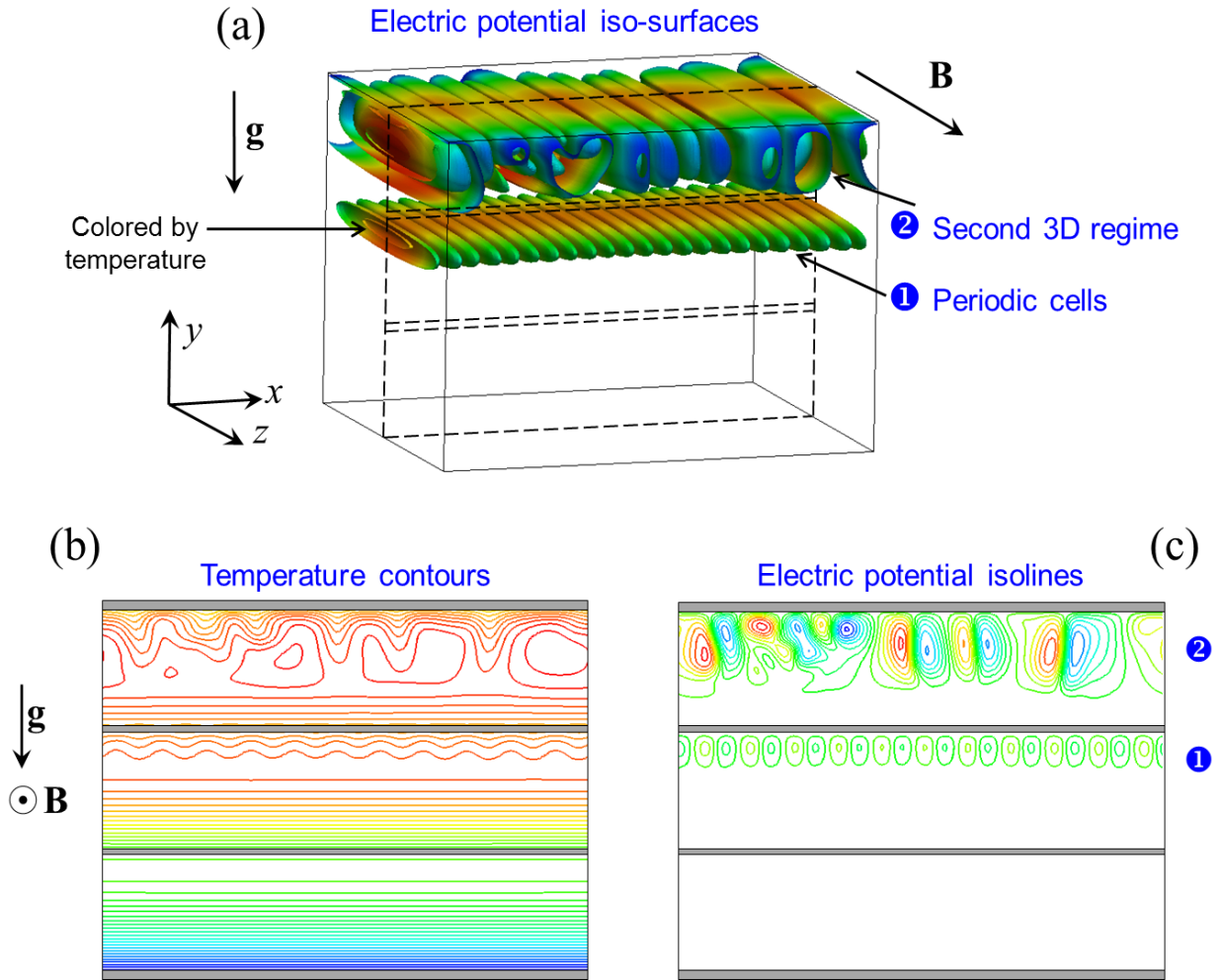


Figure 11: (a) Three dimensional isosurfaces of electric potential colored by the temperature. In the lower duct no convection sets in, in the middle channel periodic convective rolls are present as characteristic for the first 3D regime. In the upper duct irregular cells show the transition to the second 3D regime. (b) Isotherms and (c) electric potential isolines on the middle plane of the geometry at $z = 0$ for the flow at $Ha = 2000$ and $Gr_a = 2.2 \cdot 10^7$.

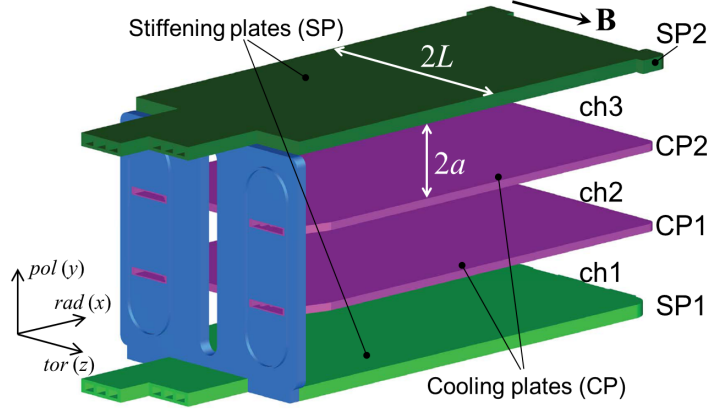


Figure 12: Breeder unit with two cooling plates and stiffening plates according to the TBM design 2009 by CEA.

step. The downward flow feeds a high velocity jet along the lower stiffening plate SP1 that promotes a stable temperature stratification in ch1. Intense convective motions that enhance the heat transfer are instead visible in ch2 and ch3. Close to the upper stiffening plate an unstable density stratification drives a significant convective circulation. In ch1 and ch2 large vertical (poloidal) temperature gradients $\partial T/\partial y$ occur and between SP1 and CP1 a temperature difference of about 40–55 degrees is established. Studies of MHD-convective flows in electrically and thermally coupled parallel channels, as ch1, ch2 and ch3, with very large radial extent, as described in section 3.1.2, have already shown that the most thermally unstable regions are those close to the upper stiffening plate (SP2) and to the second cooling plate (CP2). The lower channel ch1 is the most stable one from the thermal point of view. Contours of electric potential fluctuations, $\phi' = \phi - \bar{\phi}$, are visualized in Fig.14 for the buoyant-MHD flow with $Ha = 1000$ and $Gr_a = 0.85 \cdot 10^8$. Results highlight a typical effect of the presence of a magnetic field, i.e. the elongation of flow structures in magnetic field direction. Along magnetic field lines core-flow properties are rather uniform. Gradients tend to be localized in thin boundary layers at the Hartmann walls.

Let us now consider a realistic radial distribution of the neutron thermal load as shown in Fig.16.

In Fig.15 contours of mean electric potential are depicted for the flow at $Ha = 2000$ and $Gr_a = 1.2 \cdot 10^8$ (corresponding to an average heat source of $\bar{Q} \simeq 1.4 \text{ MW/m}^3$). In Fig.17 typical time-averaged velocity streamlines are plotted in the central vertical plane of the geometry for the flow shown in Fig.15. Four characteristic convective patterns can be identified. At the first wall the intense downward motion yields a horizontal velocity jet along the bottom stiffening plate. The fluid that reaches the back plate (BP) and moves upwards passing through the small opening between CP1 and back wall can take two different paths. It circulates towards the upper stiffening plate (red and black streamlines) or it flows between the two CPs approaching the first wall (yellow path). Near the back plate and the upper stiffening plate smaller recirculations are present as well as a large convective cell as marked by green lines. Another typical flow path is drawn in blue and it is localized near the FW.

Iso-surfaces of electric potential fluctuations ϕ' are plotted in Fig.18 for the flow at $Ha = 2000$

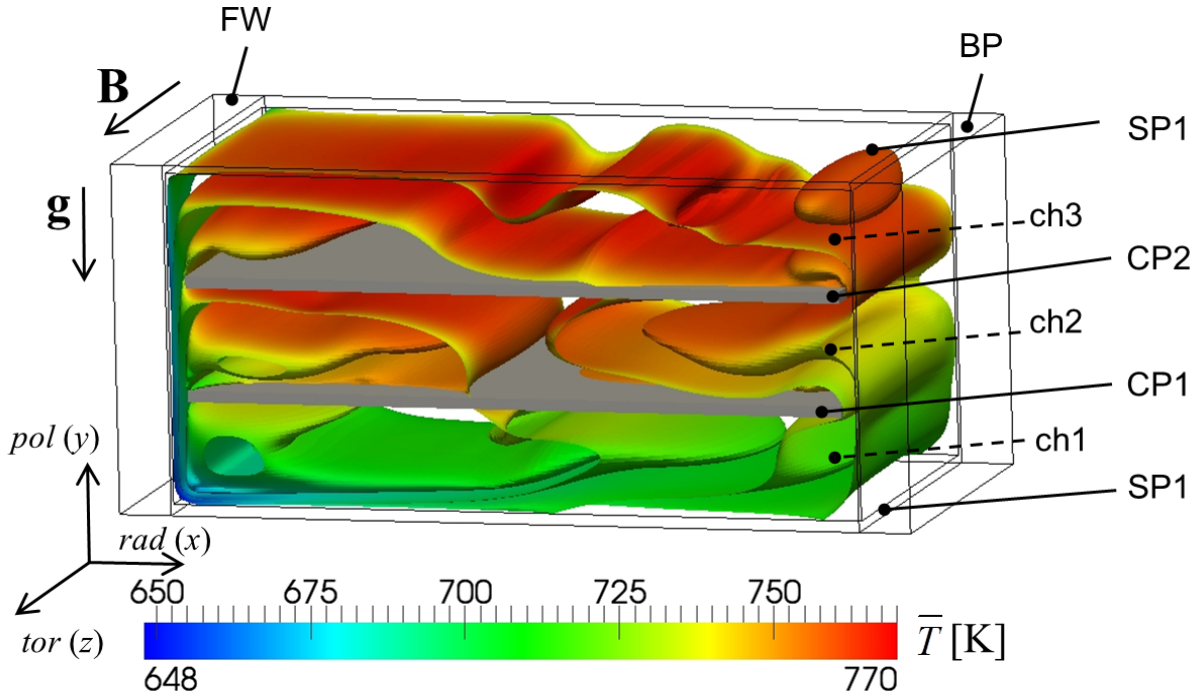


Figure 13: Iso-surfaces of time averaged electric potential for the flow at $Ha = 1000$ and uniform volumetric heat source $\bar{Q} = 1\text{MW/m}^3$ ($Gr_a = 0.85 \cdot 10^8$). The color indicates the time-averaged temperature.

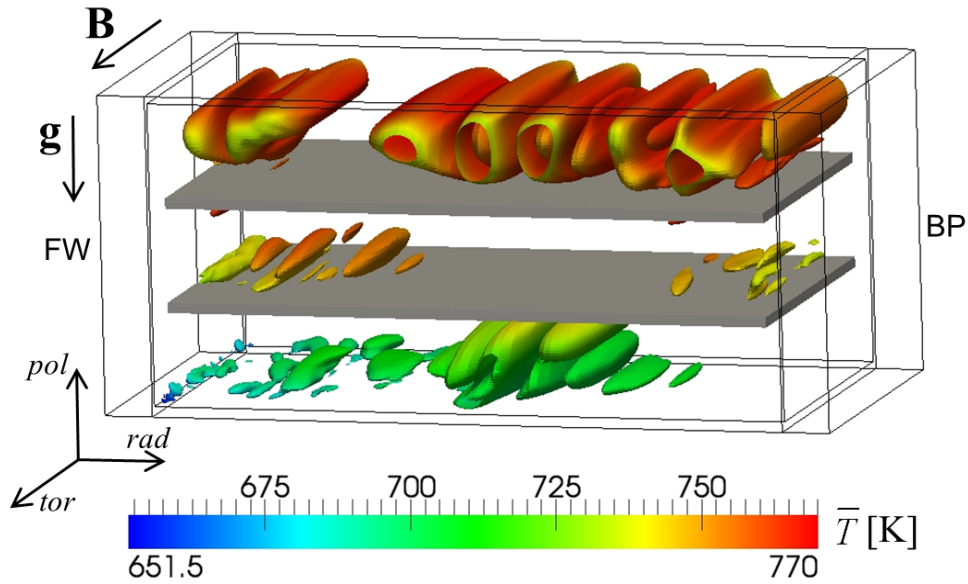


Figure 14: Iso-surfaces of electric potential fluctuations, $\phi' = \phi - \bar{\phi}$, for the flow at $Ha = 1000$ and uniform volumetric heat source $\bar{Q} = 1\text{MW/m}^3$ ($Gr_a = 0.85 \cdot 10^8$). The color indicates the time-averaged temperature.

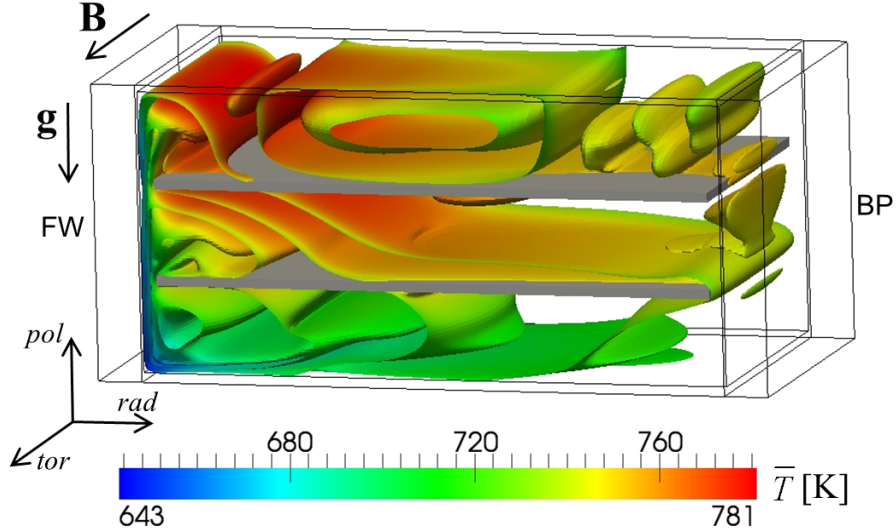


Figure 15: Iso-surfaces of time averaged electric potential, colored by averaged temperature, for $Ha = 2000$ and $Gr_a = 1.2 \cdot 10^8$. The imposed internal heat load varies in radial direction and its distribution is the result of a neutronic analysis (Villari et al. (2010)).

and non-uniform internal neutron load. Comparing the results with those visualized in Fig.14 for a constant volumetric heat source and $Ha = 1000$ it can be observed that by increasing the imposed magnetic field convective rolls elongate not only along magnetic field lines but also vertically and they become smaller in radial direction due to a stabilizing effect of the stronger electromagnetic forces.

A higher imposed magnetic field leads to a smaller velocity in the BU as shown by the distribution of time-averaged radial velocity \bar{u} in Fig.19. Here \bar{u} is plotted in the BU at four radial positions ($x = const$) for magneto-convective flows at $Ha = 2000$ and 4000 when a radially varying volumetric heat source is applied ($Gr_a = 1.2 \cdot 10^8$). Velocity jets are present at walls parallel to the magnetic field, i.e. along CP and SP. The strong velocity at the bottom of the BU originates from the descending flow along the FW. When approaching the back plate the velocity distribution is characterized by higher velocity in the parallel layers and by a rather uniform core in ch1 and ch2. Flow oscillations occur in ch3 (upper duct). For the flow at $Ha = 4000$ (Fig.19(b)) bulk velocity can be smaller than 0.3 mm/s.

The radial distribution of time averaged temperature along the central line l_c of the BU (see Fig.17) is plotted in Fig.20 for $Gr_a = 1.2 \cdot 10^8$ and different Hartmann numbers Ha . By increasing the Hartmann number, i.e. the magnitude of the applied magnetic field, the mean temperature in the fluid becomes larger due to the reduced convective motion damped by electromagnetic Lorentz forces. The temperature profile marked by a dashed line has been obtained for a case in which no convection is present ($Gr_a = 0$), i.e. conduction is the only heat transfer mechanism. It can be noticed that when the Hartmann number becomes larger the radial temperature distribution approaches asymptotically the dashed line. For that reason this limiting case has been indicated as $Ha \rightarrow \infty$. In the sub-plot in Fig.20 the time-averaged temperature is plotted along the poloidal direction in the middle of the BU for the flow at $Ha = 2000$ and $Gr_a = 1.2 \cdot 10^8$ showing that in the lower duct the temperature difference between upper and bottom walls is much larger than in the other channels.

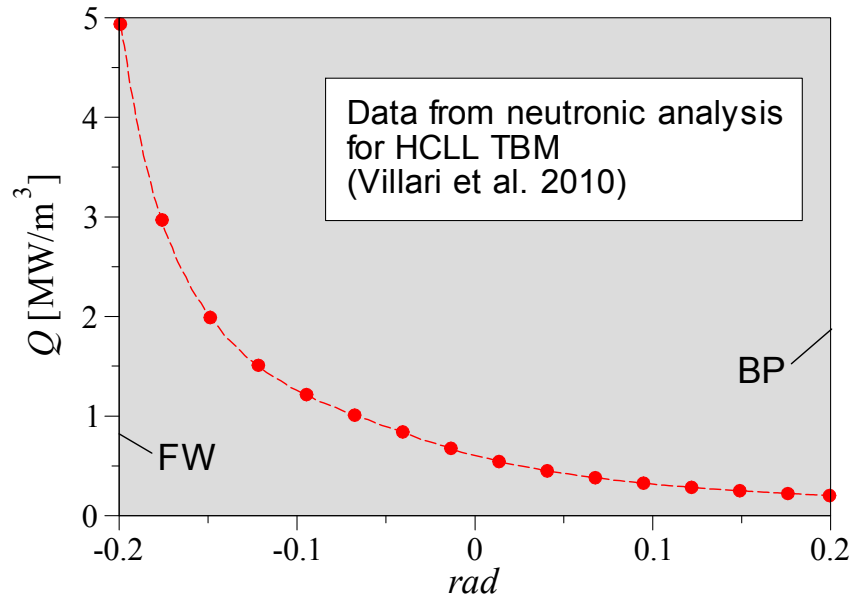


Figure 16: Radial distribution of neutron volumetric heat source as given by neutronic analyses for the HCLL TBM.

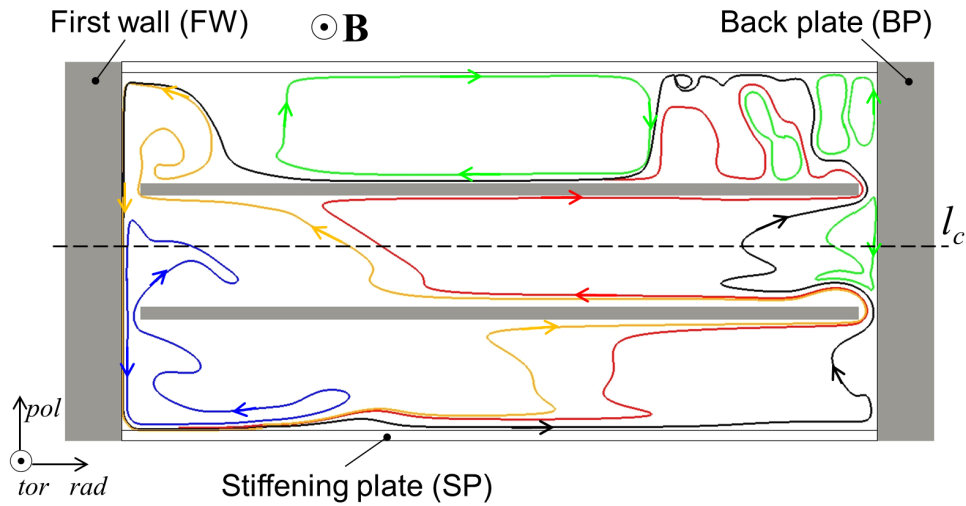


Figure 17: Sketch of typical convective patterns as present in case of a radial distribution of the neutronic load in the fluid ($Ha = 2000$, $Gr_a = 1.2 \cdot 10^8$).

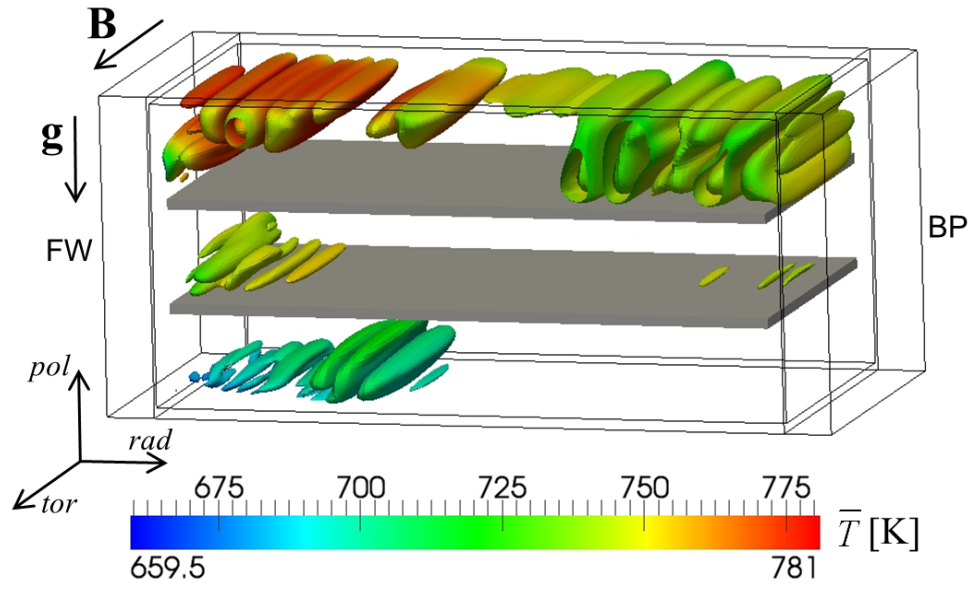


Figure 18: Iso-surfaces of electric potential fluctuations, $\phi' = \phi - \bar{\phi}$, for the flow at $Ha = 2000$ and radially varying heat load ($Gr_a = 1.2 \cdot 10^8$). Color indicates time-averaged temperature.

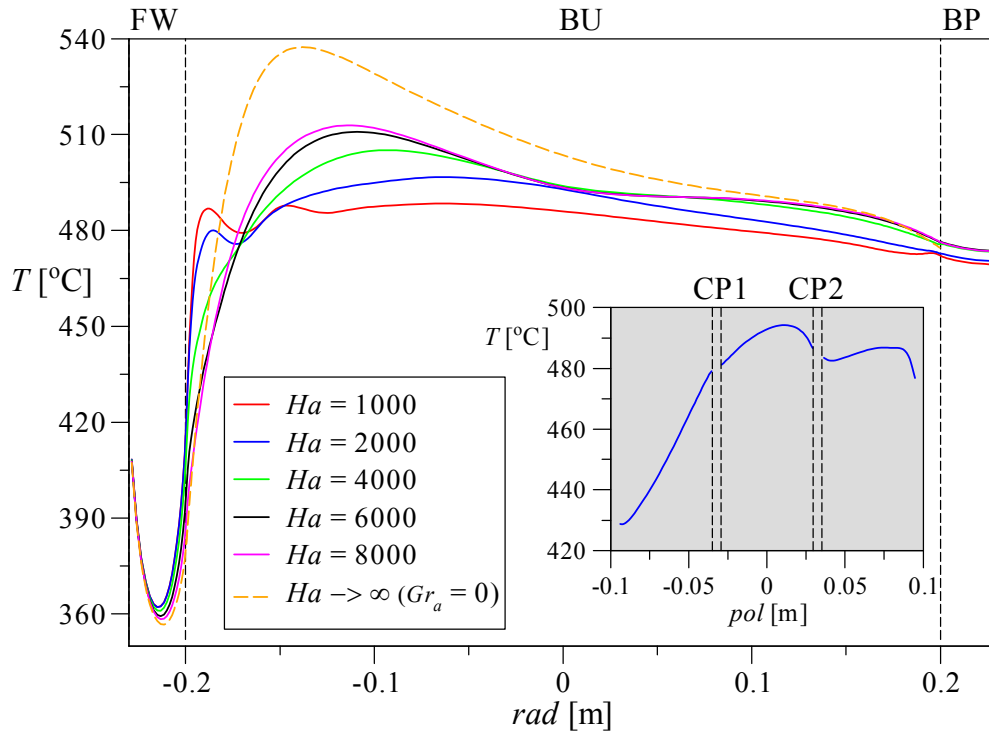


Figure 20: Radial distribution of time-averaged temperature along the central line l_c of the geometry (see Fig.17), for different Hartmann numbers Ha and an imposed radial profile of the power density ($Gr_a = 1.2 \cdot 10^8$). In the sub-plot the averaged temperature is plotted in the middle of the BU along the poloidal direction for the flow at $Ha = 2000$.

4 Conclusions

Magneto-convective flows in horizontal ducts having electrically and thermally conducting walls have been analyzed numerically for intense magnetic fields. Two configurations are considered, in a first case the flow is studied in slender channels that are infinitely extended in axial direction, a thermal source is distributed uniformly in the fluid and heat is homogeneously extracted from the walls. In a second case magneto-convective flows in a cavity are investigated, both uniform and spatially varying thermal loads are applied and the wall cooling depends on the difference between temperatures of wall and helium coolant. A model has been developed that uses an empirical correlation (Gnielinski (1975)) to simulate the heat transfer from the hot structural material into the helium flow. For both cases isotherms, flow streamlines and electric potential iso-surfaces have been studied for different internal heat sources, i.e. various Grashof numbers in the range $10^6 \lesssim Gr_a \lesssim 10^8$ corresponding to volumetric heating of about $0.04 \div 5 \text{ MW/m}^3$. A preliminary remark is required concerning the choice of the geometries and the dimensions. Since the design for a HCLL TBM is already well defined, while the one for a DEMO blanket was not available when the present work started, we took the TBM as a model geometry with the purpose of identifying the main convective patterns and phenomena occurring in a blanket breeder unit due to non-uniform thermal conditions. The next step will be understanding how the parameters typical of a DEMO reactor can modify the obtained results.

The first simplified case has been selected since it allows getting an overview of the mechanism that determines the onset of convective motions in geometries related to HCLL blankets and the way in which convective instabilities develop from periodic patterns to irregular large time dependent flow structures. It is found that when the internal heating is large enough ($Gr_a > Gr_{a,cr}$), the stable state, characterized by a parabolic vertical distribution of temperature, loses its stability and convective motion sets in as spatially periodic pairs of counter-rotating rolls. The latter ones develop with their axes aligned with the horizontal magnetic field. The number of cells depends on the intensity of the magnetic field and on the volumetric thermal load. By increasing the Grashof number instabilities, which were first localized in the upper portion of the duct, extend towards the lower wall and flow structures become larger. Three main flow regimes have been identified: a 2D stable flow where a weak convective motion driven by horizontal temperature gradients is present, a first 3D regime characterized by periodic convective rolls aligned with the magnetic field and a second 3D regime in which small structures combine to form larger cells. The transition pattern from the first to the second 3D regime is still regular but pairs of rolls elongate in vertical direction and smaller cells occur that merge to give rise to the larger structures typical of the second convective regime.

In case of three electrically and thermally coupled parallel ducts, the vertical temperature distribution is strongly asymmetric resulting in a significant temperature difference between the two horizontal stiffening plates that depends on the magnitude of the magnetic field (Ha) and the heat source (Gr_a). Noticeably different flow conditions are present in the three coupled ducts. Perturbations in the flow field first occur in the upper duct, then in the middle one and at the end in the lower channel. Instabilities start as periodic rolls along the upper stiffening plate where strong temperature gradients are present due to the fact that the SP has a more efficient cooling than the CP. The development of convective structures by increasing the volumetric heat source is analogous to the one in a single duct: periodic cells, elongated rolls, larger rotating structures, time dependent instabilities. The numerical results clearly show the importance of

thermal and electrical coupling when predicting magneto-convective flows in geometries relevant for liquid metal blanket applications and of the use of realistic electric and thermal conditions of fluid and wall materials.

The presence of a heat source that varies in radial direction, as it occurs in a breeder unit of a fusion blanket, is expected to create even more noticeable temperature variations and intense convective circulations compared to the case previously described where a homogeneous thermal load is applied. In order to investigate such operating conditions three dimensional numerical simulations have been performed for magneto-convective flows in a breeder unit of a HCLL TBM when a spatially varying power source is present. Realistic thermal and electrical properties of structural material and liquid breeder have been considered, as well as thermal operating conditions as expected in ITER (Villari et al. (2010)). The influence of the radial distribution of the neutron load in the lead lithium has been investigated for increasing strength of the applied magnetic field (Ha). The heat transfer between solid walls and helium coolant has been described by means of an empirical correlation (Gnielinski (1975)).

The non-uniform thermal conditions, caused by the neutron power density and heat extraction through the walls, result in complex convective motions in the form of rolls of different size with axes aligned with the toroidal magnetic field. The liquid metal circulates preferentially in planes perpendicular to \mathbf{B} . In all investigated cases a large convective stream is present that moves the fluid from the colder FW to the BP and to the upper stiffening plate (see e.g. the black flow path in Fig.17). Time-average convective motion and perturbations are significantly damped by increasing the magnitude of the magnetic field due to the braking action of the stronger electromagnetic forces. The observed larger mean temperature in the BU for the flow with increasing Hartmann number indicates the attenuation of the convective heat transfer in the liquid metal. Another consequence of imposing a stronger magnetic field is the reduction of the time averaged velocity in the breeder unit.

In boundary layers that form at walls parallel to the magnetic field, i.e. along cooling and stiffening plates, high-velocity jets occur. At the FW an intense downwards flow is present due to the significant cooling of this wall yielding the formation of a cold velocity jet that enters the lower channel. As a consequence, a stable density stratification is established below CP1 with a large temperature difference between SP1 and CP1. For flows at $Ha = 2000$ this difference can be of the order of 45 – 55 degrees (see sub plot in Fig.20). This strong temperature gradient is most likely reduced if the thermal coupling of adjacent breeder units in a column of a TBM is considered. This will be analyzed in future work.

In planned numerical studies a neutron thermal load will be applied also inside the duct walls and this should mitigate partly the significant temperature reduction across the first wall that is caused by its strong cooling. Definition of the physical properties of helium and wall materials as a function of temperature should also be taken into account.

References

- Aiello, G., de Dinechin, G., Forest, L., Gabriel, F., Li Puma, A., Rampal, G., Rigal, E., Salavy, J. and Simon, H.: 2011, HCLL TBM design status and development, *Fusion Engineering and Design* **86**(9-11), 2129–2134.
- Aiello, G., Gabriel, F., Rampal, G. and Salavy, J.-F.: 2009, A new cooling scheme for the HCLL TBM, *Fusion Engineering and Design* **84**, 390–393.
- Ben Hadid, H. and Henry, D.: 1997, Numerical study of convection in a horizontal Bridgman configuration under the action of a constant magnetic field. Part 2. Three-dimensional flow, *Journal of Fluid Mechanics* **333**, 57–83.
- Bühler, L.: 1998, Laminar buoyant magnetohydrodynamic flow in vertical rectangular ducts, *Physics of Fluids* **10**(1), 223–236.
- Burr, U. and Müller, U.: 2002, Rayleigh-Bénard convection in liquid metal layers under the influence of a horizontal magnetic field, *Journal of Fluid Mechanics* **453**, 345–369.
- Gabriel, F., Escuriol, Y., Dabbene, F., Gastaldi, O., Salavy, J. and Giancarli, L.: 2007, A 2D finite element modelling of tritium permeation for the HCLL DEMO blanket module, *Fusion Engineering and Design* **82**(15-24), 2204–2211.
- Gelfgat, A. Y. and Molokov, S.: 2011, Quasi-two-dimensional convection in a three-dimensional laterally heated box in a strong magnetic field normal to main circulation, *Physics of Fluids* **23**(3), 034101–1–13.
- Gnielinski, V.: 1975, Neue Gleichungen für den Wärme- und den Stoffübergang in turbulent durchströmten Rohren und Kanälen, *Forschung im Ingenieurwesen A* **41**, 8–16.
- Hjellming, L. N. and Walker, J. S.: 1987, Melt motion in a Czochralski crystal puller with an axial magnetic field: motion due to buoyancy and thermocapillarity, *Journal of Fluid Mechanics* **182**, 335–368.
- Jauch, U., Karcher, V., Schulz, B. and Haase, G.: 1986, Thermophysical properties in the system Li-Pb, *Technical Report KfK 4144*, Kernforschungszentrum Karlsruhe.
- Kharicha, A., Molokov, S., Aleksandrova, S. and Bühler, L.: 2004, Buoyant convection in the HCLL blanket in a strong uniform magnetic field, *Technical Report FZKA 6959*, Forschungszentrum Karlsruhe.
- LiPuma, A., Aiello, G. and Morin, A.: 2010, Design description document of the reference option for the HCLL In-TBM breeder unit, *Technical Report DEN/DANS/DM2S/SERMA/LPEC/RT/10-4921/A*, CEA.
- Mas de Les Valls, E., Batet, L., de Medina, V., Fradera, J. and Sedano, L.: 2011, Modelling of integrated effect of volumetric heating and magnetic field on tritium transport in a U-bend flow as applied to HCLL blanket concept, *Fusion Engineering and Design* **86**(4-5), 341–356.

- Mas de les Valls, E., Batet, L., de Medina, V. and Sedano, L. A.: 2012, MHD thermofluid flow simulation of channels with a uniform thermal load as applied to HCLL breeding blankets for fusion technology, *Magnetohydrodynamics* **48**(1), 157–168.
- Mergia, K. and Boukos, N.: 2008, Structural, thermal, electrical and magnetic properties of Eurofer 97 steel, *Journal of Nuclear Materials* **373**, 1–8.
- Mistrangelo, C. and Bühler, L.: 2008, Electric flow coupling in the HCLL blanket concept, *Fusion Engineering and Design* **83**, 1232–1237.
- Mistrangelo, C. and Bühler, L.: 2011, Development of a numerical tool to simulate magnetohydrodynamic interactions of liquid metals with strong applied magnetic fields, *Fusion Science and Technology* **60**(2), 798–803.
- Ni, M.-J., Munipalli, R., Morley, N. B., Huang, P. and Abdou, M. A.: 2007, A current density conservative scheme for incompressible MHD flows at a low magnetic Reynolds number. Part I: On a rectangular collocated grid system, *Journal of Computational Physics* **227**(1), 174–204.
- Ozoe, H. and Okada, K.: 1989, The effect of the direction of the external magnetic field on three-dimensional natural convection in a cubical enclosure, *International Journal of Heat and Mass Transfer* **32**(10), 1939–1954.
- Rampal, G., Aiello, G. and Li Puma, A.: 2009, Input data, software/models, physical correlations and material properties for HCLL TBM generic box and shield design activities, *Technical Report DM2S SEMT/BCCR/RT/09-020/A*, CEA.
- Salavy, J.-F., Aiello, G., David, O., Gabriel, F., Giancarli, L., Girard, C., Jonquieres, N., Laffont, G., Madeleine, S., Poitevin, Y., Rampal, G., Ricapito, I. and Spichal, K.: 2008, The HCLL Test Blanket Module system: Present reference design, system integration in ITER and R&D needs, *Fusion Engineering and Design* **83**, 1157–1162.
- Sawan, M. E., Marriott, E. P. and Dagher, M.: 2009, Neutronics performance parameters for the US dual coolant lead lithium ITER test blanket module, *Proceedings of 23rd IEEE/NPSS Symposium on Fusion Engineering (SOFE)*.
- Tavassoli, F.: 2004, Fusion demo interim structural design criteria (DISDC) - appendix A Material design limit data - a3.s18e Eurofer steel, EFDA TASK TW4-TTMS-005-D01, *Technical Report DMN/DIR/NT/2004-02/A*, CEA.
- Vetcha, N., Smolentsev, S., Abdou, M. and Moreau, R.: 2013, Study of instabilities and quasi-two-dimensional turbulence in volumetrically heated magnetohydrodynamic flows in a vertical rectangular duct, *Physics of Fluids* **25**, 024102.
URL: <http://dx.doi.org/10.1063/1.4791605>
- Villari, R., Petrizzi, L. and Moro, F.: 2010, Neutronic analysis for HCLL TBM preliminary design phase, *Technical report*, ENEA.



ISSN 1869-9669
ISBN 978-3-7315-0226-5

ISBN 978-3-7315-0226-5



9 783731 502265 >